Analysis of radiation modeling for turbulent combustion : development of a methodology to couple turbulent combustion and radiative heat transfer in LES

POITOU Damien
CERFACS
42, Avenue Gaspard Coriolis
31057 Toulouse Cedex 01
France.
Email : poitou@cerfacs.fr

EL HAFI Mouna
Centre RAPSODEE
École des Mines d'Albi
Campus Jarlard
81013 ALBI
France

CUENOT Bénédicte
CERFACS
42, Avenue Gaspard Coriolis
31057 Toulouse Cedex 01
France.

ABSTRACT

Radiation exchanges must be taken into account to improve Large Eddy Simulation (LES) prediction of turbulent combustion, in particular for wall heat fluxes. Because of its interaction with turbulence and its impact on the formation of polluting species, unsteady coupled calculations are required. This work constitutes a first step towards coupled LES-radiation simulations, selecting the optimal methodology based on systematic comparisons of accuracy and CPU cost. Radiation is solved with the Discrete Ordinate Method (DOM) and different spectral models. To reach the best compromise between accuracy and CPU time, the performance of various spectral models and discretizations (angular, temporal and spatial) is studied. It is shown that the use of a global spectral model combined with a mesh coarsening (compared to the LES mesh) and a minimal coupling frequency N_{it} allows to compute one radiative solution faster than N_{it} LES iterations, while keeping a good accuracy. It also appears than the impact on accuracy of the angular discretization in the DOM is very small compared to the impact of the spectral model. The determined optimal methodology may be used to perform unsteady coupled calculations of turbulent combustion with radiation.

Introduction

Radiation is one important heat transfer phenomenon in combustion devices. Previous studies have shown that is is necessary to solve radiative heat transfer to improve combustion simulation results [1, 2, 3]. Heat losses may change the temperature of the flame by more than 100 K which can significantly modify the chemical kinetics, cf. polluting species like NO_x, CO, or soot particles in luminous flames. Moreover, the radiative heat flux must be determined to evaluate correctly the thermal exchanges with walls. Due to the complexity of radiation and the nonlinear interactions between reacting flows, heat transfer and turbulence perform coupled simulations in practical situations is a challenge.

While Reynolds Average Navier-Stokes (RANS) provide only averaged results, Large Eddy Simulation (LES) [4, 5] is able to predict instantaneous flow characteristics. Also, LES is in principle more accurate as the large flow scales are resolved explicitly while only the small scales are modeled. Many authors demonstrated the advantages of LES in application to gas turbine engines [6], laboratory flames [7] or in other combustion systems [8, 9].

Radiation may be calculated from a steady flame solution to study wall heat fluxes for example. However the interaction with the turbulence may have a strong impact on radiation : this is referred as the Turbulence-Radiation Interaction (TRI)

problem which has been studied by many authors (see [10] for a review on this topic). To take into account the interaction with turbulence and chemistry coupled calculations are required.

Literature about radiation in LES is limited. Only few papers present detailed radiation calculations in configurations involving a high number of mesh cells (more than a million). Desjardin *et al.* [11] have coupled combustion and radiation in a bi-dimensional configuration of a non-premixed acetylene/air planar jet flame with 16 000 cells. The gas is transparent and only the absorption of soot is considered. The radiative transfer is solved in a finite volume approach using the Discrete Ordinate Method (DOM). Jones *et al.* [12] have also used DOM with S_n quadratures in a LES of a gas turbine combustor using a 16 000 cells mesh and a gray gas spectral model. Joseph *et al.* [13] developed a DOM solver for unstructured meshes to compute radiation in the PRECCINSTA burner [14] where the swirled flames is typical of turbo-engines. The mesh contained 138 000 cells and a narrow band model (SNBcK) was used. However the radiation and LES calculation were not coupled. More recently Dos Santos *et al.* [3, 15] worked on the feasibility of the coupling between turbulent combustion and detailed radiation in practical systems. First a 2D situation has been studied in [15] using a raytracing method. Then a 3D premixed propane/air flame stabilized behind a triangular flame holder [16, 17] was calculated with coupled DOM-LES approaches [3]. Preliminary results demonstrated the feasibility of the coupling and showed first trends of the impact of radiation on flame dynamics. Due to the very high computing cost of both LES and radiation simulations, further investigation is needed to optimize the choice of the models and their coupling to provide a good compromise between CPU time and accuracy.

The main objective of this work is to propose an efficient and accurate radiation solver adapted to LES. This means in particular that the ratio between CPU time of DOM and LES must be close to 1. This will be achieved by an optimal choice of models and parameters, such as the radiative properties model, the subcycling frequency, the mesh resolution, the distribution over parallel processors or the number of directions to discretize the solid angle in DOM.

In the following, section one describes the test configuration which is the same as in [3, 15]. Then, the LES calculation of this configuration is briefly presented. In the second section, the numerical method and radiation models are detailed. The approach to couple combustion with radiation is presented in the third section where a subcycling scheme is defined. In section four, the influence of the physical and numerical parameters of the radiation model is studied and analyzed to determine the best compromise between calculation time and accuracy. In particular the influence of the angular discretization and of the spectral model are discussed. In section five the effect of the mesh resolution on radiation results is investigated whereas in section six the influence of the wall reflection is addressed. Finally the impact of all parameters on the radiative time calculation with the associated level of accuracy is summarized and compared to the combustion calculation time.

1 The test configuration

1.1 Geometry

The test configuration was initially set up and studied experimentally by Knikker *et al.* [16, 17, 7] and is represented in Fig. 1.

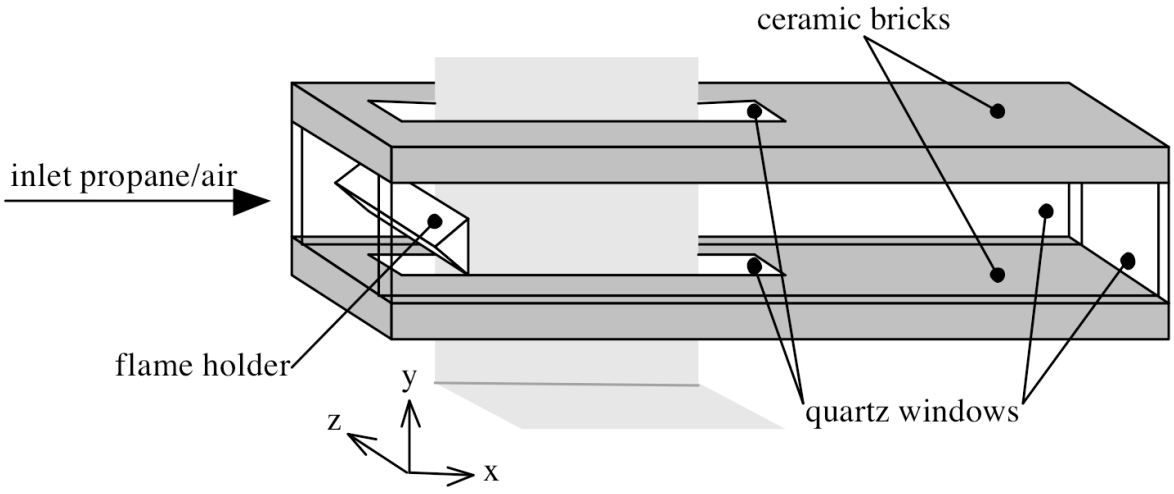

Fig. 1. Test configuration [16].

A premixed propane/air flow is injected into a rectangular combustor. The dimensions of the combustion chamber in

Parameters	α_i	β_i	A_i(cgs)	E_{a_i}(cal.mol^{-1})
Reaction (I)	$+0.9028$	$+0.6855$	$+2.0\times10^{12}$	33 000.0
Reaction (II)	$+1.0$	$+0.50$	-4.5×10^{10}	12 000.0

Table 1. Two-steps chemical mechanism parameters for propane/air flames.

height, depth and length are respectively 50, 80 and 300 mm. Lateral walls are transparent artificial quartz windows for visualisation of the flame. The upper and the lower walls are made of ceramic material for thermal isolation, including quartz windows used to introduce LASER sheets for measurements (cf. Fig. 1).

A stainless steel triangular flame holder is embedded in the lateral windows. The height is 25 mm corresponding to a 50% blockage ratio. The V-shaped turbulent flame is stabilized by the hot gases recirculating behind the flame holder. This configuration was originally set up to validate LES numerical models. It is a good candidate for the present work as it contains all the ingredients to be tested : unsteady flame, measurements, ...

Some different cases exist depending on the inlet velocity and the equivalence ratio. The present case corresponds to an inlet velocity of 5 m.s^{-1} and an equivalent ratio of $\phi = 1$ (turbulence level about 5%).

1.2 LES calculation

The numerical calculation was conducted with AVBP[1]. It is a compressible Navier-Stokes solver using finite volume and a 3$^{\text{rd}}$ order Runge-Kutta temporal scheme. Two spatial integration schemes are available : a 2$^{\text{nd}}$ order (Lax-Wendroff) and a 3$^{\text{rd}}$ order (TTGC [18]) scheme. Velocity, energy and species conservation equations are solved using realistic thermo-chemistry.

The subgrid model describing the turbulent stress tensor is based on the turbulent viscosity of the WALE model [19, 20]. Turbulent fluxes for thermal diffusion and species are modeled by classical gradient laws. Turbulent combustion is represented by the Thickened Flame Model (TFLES [21]) which artificially increases the number of mesh points inside the flame front without altering the flame speed. Subgrid wrinkling is modeled using an efficiency function [21].

The chemistry of propane/air combustion is represented by a two-steps mechanism [22] :

$$\begin{aligned} C_3H_8 + \frac{7}{2}O_2 &\Rightarrow 3CO + 4H_20 \\ CO + \frac{1}{2}O_2 &\Leftrightarrow CO_2 \end{aligned} \tag{1}$$

The corresponding reaction rates are given by :

$$\dot{\omega}_1 = A_1[C_3H_8]^{\alpha_1}[O_2]^{\beta_1}\exp(-E_{a_1}/RT) \tag{2}$$

$$\dot{\omega}_2 = A_2[CO_2]^{\alpha_2}[O_2]^{\beta_2}\exp(-E_{a_2}/RT) \tag{3}$$

where $[X]$ is the mass fraction of specie X and α_i, β_i are fitted coefficients different from the stoechiometric coefficients, A_i is the pre-exponential factor and E_{a_i} is the activation energy. They are given in Table 1. These values lead to a laminar flame speed $s_l^0 = 0.48$ m.s^{-1} for an equivalent ratio of $\Phi = 1$. The filtered reaction rates $\overline{\dot{\omega}_i}$ are calculated from Eqs. 2 and 3 using filtered values of the mass fractions and temperature and the TFLES approach. In the present configuration, the maximal thickening factor is $F_{max} = 20$ indicating a correct behaviour of the model.

The calculation domain corresponds to a section of the experimental set-up (Fig. 1) and a 3D box of $30\times30\times30$ cm. The inlet starts 10 cm upstream the flame holder and the chamber is 60 cm long. The mesh contains about 4.7 millions tetrahedra, of smallest size about $\Delta = 1$ mm close to the obstacle and then increasing progressively towards the exit of the chamber (Fig. 2). To guarantee a non-disturbing outlet boundary condition, a large box with an azote coflow is added at the end of the domain. Boundary conditions are the NSCBC [23] allowing to fix a static pressure at the oulet with limited reflexion of acoustic waves in the domain.

Inlet conditions are given for the propane/air flow with a velocity of 5 m.s^{-1}, a temperature of 300 K with an equivalent

[1] http://www.cerfacs.fr/4-26334-The-AVBP-code.php

ratio of $\phi = 1$. The coflow conditions give a velocity of 20 m.s^{-1} and a temperature of 1900 K corresponding to the burnt gases temperature.

Thermal wall boundary conditions are critical and a weak point in the present simulation. The walls are not isothermal but the wall temperature is the result of thermal transfer in the solid to reach a correct wall temperature. In the present simulation this is modelled with a wall thermal resistivity of $R_{th} = 0.096$ K.m^2.W^{-1} for ceramic walls (upper and lower), $R_{th} = 0.086$ K.m^2.W^{-1} for quartz windows (front and behind) and $R_{th} = 120$ K.m^2.W^{-1} for the flame holder [3]. The walls around the atmosphere at the end of the chamber are adiabatic slip walls.

However the wall temperature is still unknown in the uncoupled radiation calculations, and assumed to be cold at $T_w = 300$ K except the walls of the atmospheric box at 1900 K. These temperatures are arbitrarily fixed as no measurements are available and may lead to an overestimation of radiative heat losses because the real wall temperature is higher than 300 K. The correct radiative loss would be obtained by coupling solid thermal transfer with the flow and radiation solver [24]. However it is assumed that it will not impact our conclusion concerning model and discretization choices.

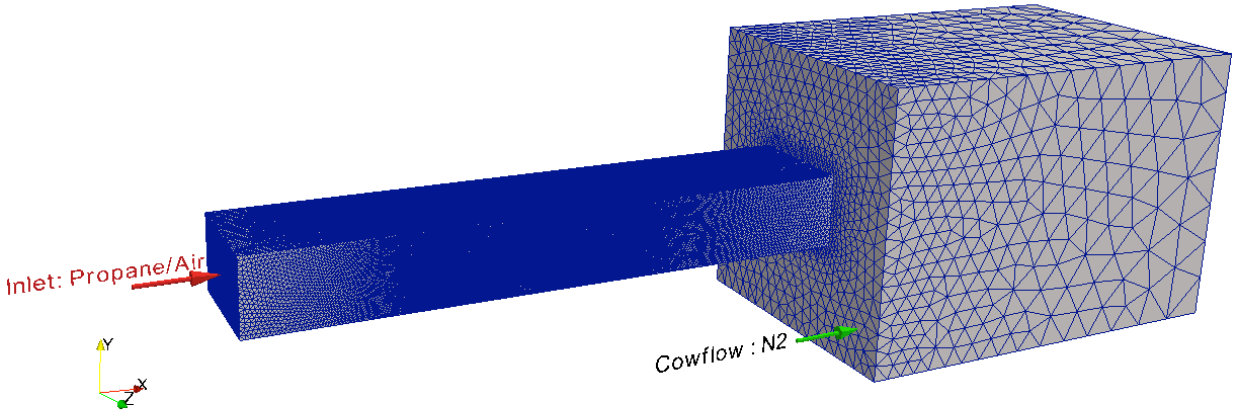

Fig. 2. Mesh used for LES.

The origin of the coordinates system is fixed at the center of the obstacle. Profiles will be plotted along 3 axes defined in Fig. 3.: the central x axis, a transversal y axis at $x = 9$ cm and an x axis close to the wall at $y = 2.5$ cm.

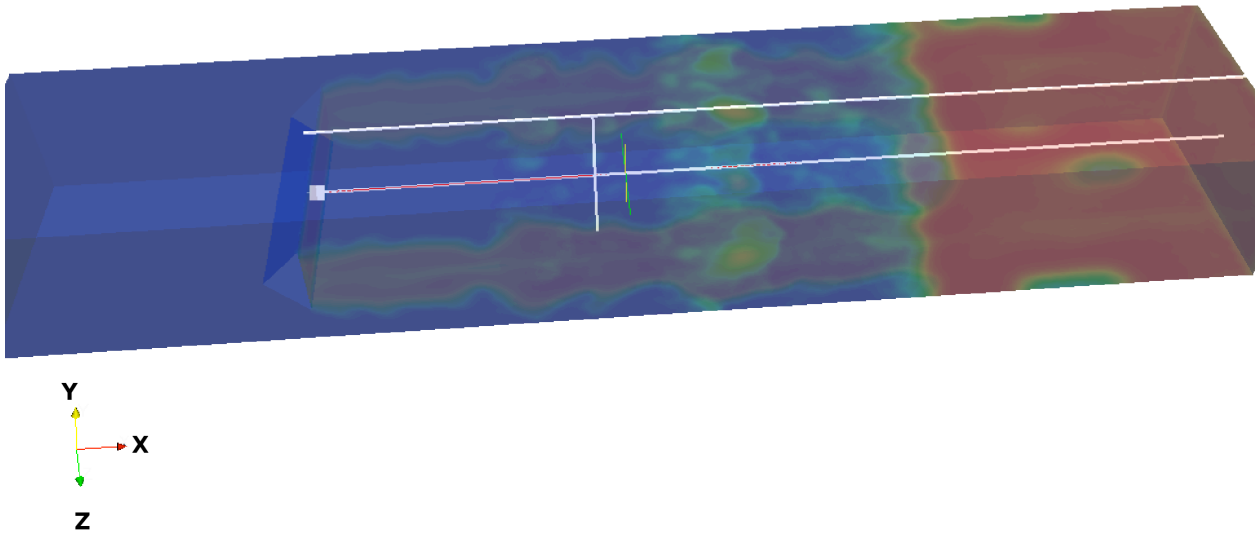

Fig. 3. Coordinates system and axis along which profiles are plotted.

1.3 LES results

Fig. 4 shows instantaneous fields of velocity magnitude, heat release and temperature from the LES calculation in the plane $y = 0$. The velocity field shows the flow structure with a recirculation zone behind the flame holder where hot gases are trapped to stabilize the flame. The instantaneous heat release illustrates the flame structure showing two branches of the reacting zone attached to the flame holder and wrinkled by the turbulence. Note that in $x = 16$cm the flame quenches on the walls before reigniting to consume the remaining fuel. The total energy released by the combustion in the chamber is 70.93 kW.

In this flame the total radiative energy is about 1.3 kW while the total heat release of combustion is close to 70 kW, i.e. the radiative loss represents only a few percents of the combustion energy. The radiative effect on the flame is therefore a second order effect. However previous studies [15, 3] have shown that radiation may have more important effects, especially by increasing the mean flow fluctuations.

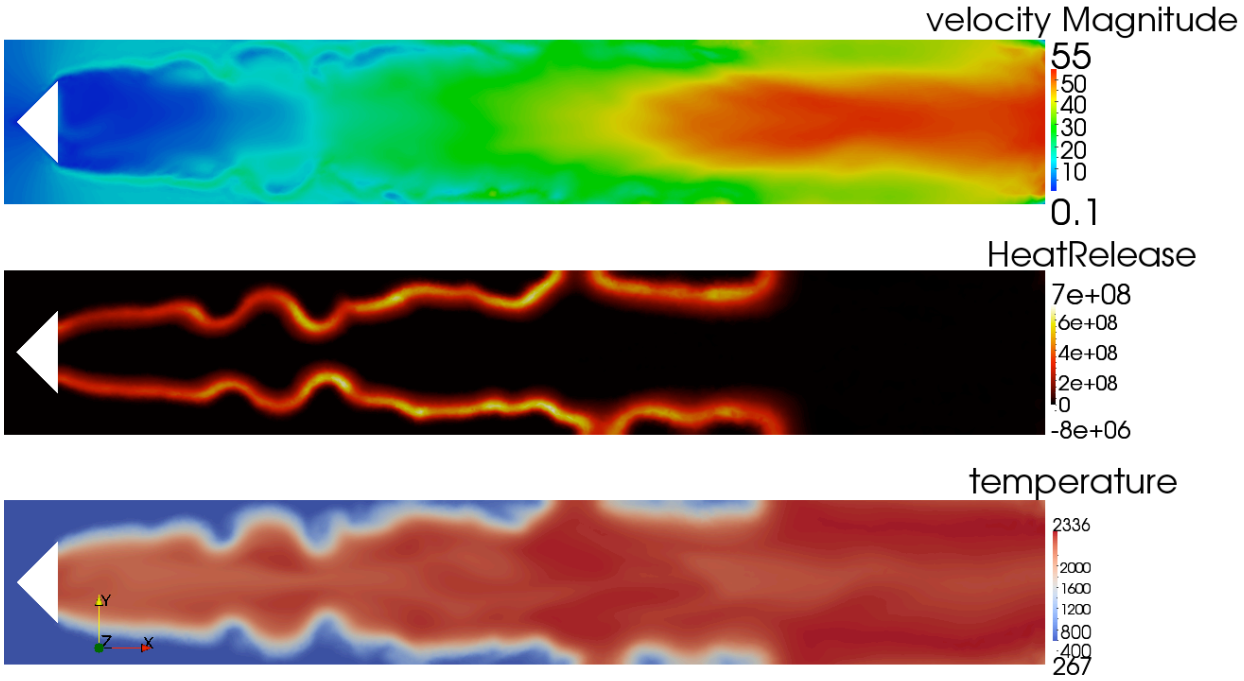

Fig. 4. Instantaneous field of temperature, heat release and magnitude velocity in the plane $y = 0$.

As the flame is artificially thickened by the combustion model TFLES the optical thickness of the flame front may be changed. However Poitou *et al.* [25] has shown that this effect is small and these results will be discussed in a future paper.

2 Modeling of the radiative heat transfer

To consider radiative heat transfer in the previous LES, a radiative source term S_r is calculated using the Radiative Transfer Equation (RTE). The differential RTE for a non scattering medium is given by :

$$\mathbf{s} \cdot \nabla L_\nu(\mathbf{x}, \mathbf{u}) = \kappa_\nu \left[L_\nu^0(\mathbf{x}) - L_\nu(\mathbf{x}, \mathbf{u}) \right] \tag{4}$$

where ν is the wavenumber, $L_\nu(\mathbf{x}, \mathbf{u})$ is the incident intensity at the point $\mathbf{x}$ in the direction $\mathbf{u}$ and κ_ν is the absorption coefficient.

The associated boundary conditions are :

$$L_\nu(\mathbf{x}_w, \mathbf{u}) = \underbrace{\varepsilon_\nu(\mathbf{x}_w) L_\nu^0(\mathbf{x}_w)}_{\text{Emitted part}} + \underbrace{\rho_\nu(\mathbf{x}_w) L_{\nu,incident}(\mathbf{x}_w, \mathbf{u})}_{\text{Reflected part}} \tag{5}$$

where $\varepsilon_\nu(\mathbf{x}_w)$ is the wall emissivity and$\rho_\nu(\mathbf{x}_w)$ the wall reflectivity ($\rho_\nu(\mathbf{x}_w) = 1 - \varepsilon_\nu(\mathbf{x}_w)$).

The source term S_r results from a double integration of the RTE in the physical and spectral spaces, leading to a macroscopic source term which depends only on the position $\mathbf{x}$:

$$S_r(\mathbf{x}) = \int_0^\infty \kappa_\nu \left[4\pi L_\nu^0(\mathbf{x}) - \int_{4\pi} L_\nu(\mathbf{x},\mathbf{u}) d\Omega \right] d\nu \tag{6}$$

2.1 Angular discretization

Various methods exist to perfom the angular integration over the discretized directions $\mathbf{u}_i$: Ray tracing methods following optical paths, P_1 methods uses spherical harmonics, Monte-Carlo methods calculate photon statistics with a high number of absorption/diffusion events, ... Here the Discrete Ordinate Method (DOM) is used which is a finite volume formulation of the RTE and offers a good compromise between accuracy and CPU time [26, 27, 14].

The radiative solver used in this work is PRISSMA[2] [26, 2, 13, 27, 25]. The RTE is solved for a set of N_{dir} directions (ordinates), computing the integral over each ordinate by a numerical quadrature :

$$\int_{4\pi} f(\mathbf{u}) d\Omega \simeq \sum_{i=1}^{N_{dir}} w_i^a f(\mathbf{u}_i) \tag{7}$$

where $\mathbf{u}_i$ are the discrete directions and ω_i^a the associated weights of S_n quadratures determined from Truelove [28].

2.2 Spectral model

The spectral dependency of the radiation is known for absorbing gases such as CO, CO_2 and H_2O and is very complex. Line-by-line model gives the absorption for each frequency which implies rhe resolution of the RTE for at least one million frequencies in each direction. Narrow-band models such as SNBcK [29] offer a good accuracy with less calculations. Goutière *et al.* have shown that the SNBcK model is very precise in combustion applications [29, 30]. Finally global models allow to reduce the calculation to 3 to 15 spectral integrations in each direction.

In PRISSMA a series of spectral models are available. The SNBcK model is implemented with 371 narrow bands of width $\Delta\nu_i$ over the IR spectrum (wavelength in the range $\lambda = [0.5; 68\ \mu\text{m}]$): 367 bands from the SNB database from [31] more 4 bands in the visible for the radiation of soot. In each narrow band the Planck function is assumed to be constant. A re-arrangement called *k*-distribution allows to calculate the absorption coefficient in each band (i) with a Gauss-Legendre quadrature (over N_q points) of the cumulative function of the possible values of absorption. The final expression of the radiative source term is then :

$$S_r(\mathbf{x}) \simeq \sum_{i=1}^{N_{band}} \Delta\nu_i \left[\sum_{j=1}^{N_{quad}} \omega_j \kappa_{ij} \left(4\pi \overline{L^0_{\Delta\nu_i}(\mathbf{x})} - \sum_{k=1}^{N_{dir}} \omega_k^a L_{ij}(\mathbf{x},\mathbf{u}_k) \right) \right] \tag{8}$$

where ω_j are the weights of the Gauss-Legendre quadrature, $\overline{L^0_{\Delta\nu_i}(\mathbf{x})}$ is the mean value of the Planck function on the i$^{\text{th}}$ narrow band, κ_{ij} and L_{ij} are respectively the absorption coefficient and the incident intensity for the quadrature point j in the i$^{\text{th}}$ band.

Typically 5 quadrature point are used, corresponding to $371 \times 5 = 1\,800$ integrations for each direction. The associated calculation time is still high and the SNBcK model is used here as a reference solution.

Two global models are also implemented in PRISSMA : the Weighted Sum of Gray Gases (WSGG) model [32] and the Full Spectrum SNBcK (FS-SNBcK) model [33, 34]. Such models are fast but their accuracy must be carefully checked.

A previous study has shown the validity limits for the global model FS-SNBcK [34] for combustion applications. For this model the macroscopic source term S_r is given by :

$$S_r(\mathbf{x}) \simeq \sum_{j=1}^{N_q} \omega_j \kappa_j \left(4\sigma T^4(\mathbf{x}) - \sum_{k=1}^{N_{dir}} \omega_k^a L_j(\mathbf{x},\mathbf{u}_k) \right) \tag{9}$$

where ω_j are the weights of the Gauss-Legendre quadrature over the full spectrum.

---

[2] PRISSMA: Parallel RadIation Solver with Spectral integration on Multicomponent mediA, `http://www.cerfacs.fr/prissma`

This model is equivalent to the WSGG approach, using a partial intensity L_j with the absorption coefficient κ_j for each quadrature point j. With the FS-SNBcK model the gray gas j is reconstructed from the narrow band properties [34]. The WSGG model suffers from an important lack of accuracy, near high gradients of temperature. Moreover it uses assumptions such as constant ratio for CO_2/H_2O, no absorption of CO, ... which may be not correct. However it represents a reference as the shortest calculation time model.

3 Coupling approach

3.1 Description of the coupling

In a coupled calculation, the radiative source term S_r must be known in the fluid solver while the radiative solver needs inputs such as the temperature, pressure and molar fractions of radiating species (H_2O, CO_2, CO and possibly soot) from the flow solver.

Fig. 5 shows how the data can be exchanged between the two codes [35, 36]. In the Sequential Coupling Strategy (SCS, Fig. 5a), all the computing resources are allocated alternatively to each of the two codes. An alternative is the Parallel Coupling Strategy (PCS) where both solvers run simultaneously sharing computational resources and using the data obtained at the previous coupling iteration (Fig. 5b).

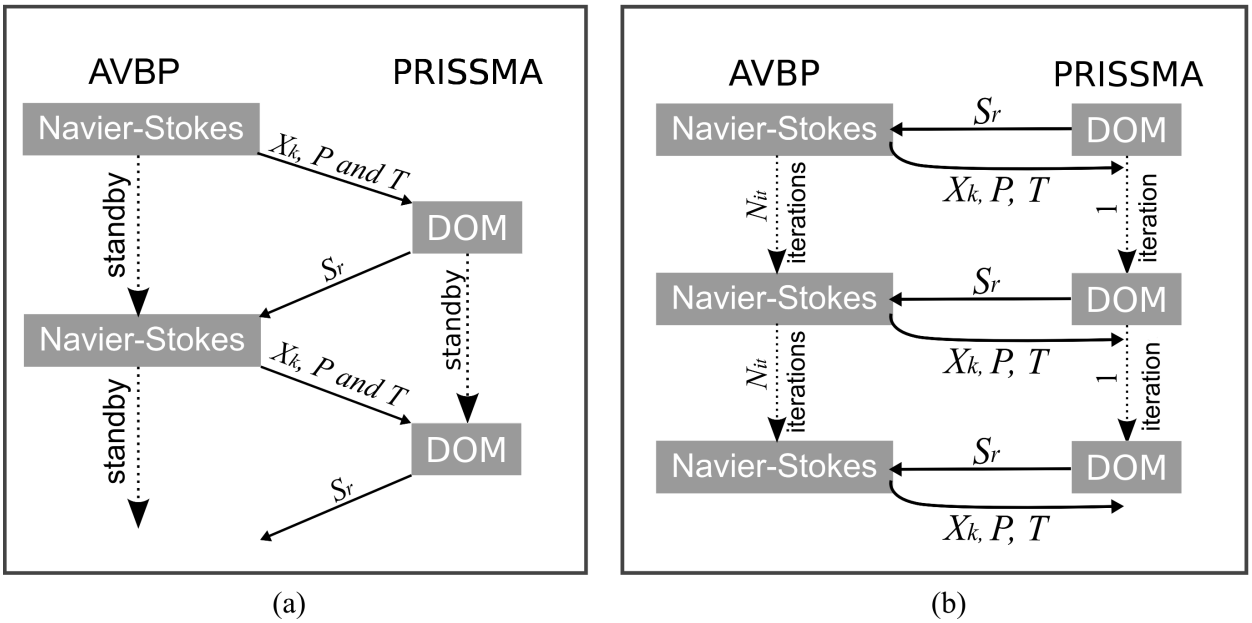

Fig. 5. (a) Sequential Coupling Strategy (SCS) and (b) Parallel Coupling Strategy (PCS).

In the present work the PCS was used, this however requires both an appropriate physical time and CPU time synchronisation [35, 36].

3.2 Physical time synchronisation

Radiation is an instantaneous phenomenon compared to fluid time scales and adapts instantaneously to the flow time evolution. Therefore is evolves with the same time scale. This time scale τ_f is not the LES time step Δt_{LES}, which corresponds to an acoustic time scale. It is convenient to introduce a coupling frequency $1/N_{it}$ where N_{it} is the number of LES iterations between two radiation calculations. Ideally $N_{it} \times \Delta t_{LES} = \tau_f$. The LES time step Δt_{LES} is fixed by the CFL criterion for the propagation of acoustic waves :

$$\Delta t_{LES} = \frac{\text{CFL} \times \Delta x_{min}}{c_s} \tag{10}$$

where Δx_{min} is the smallest mesh size and c_s is the speed of sound. In AVBP, using the 3rd order scheme [18], CFL= 0.7. For the studied configuration $\Delta t_{LES} \approx 2\ \mu s$.

The radiative source term changes with the convection of hot gas [37] and Wang [38]. The flow time scale is evaluated as:

$$\tau_f = \frac{\Delta x_{min}}{\overline{u}} \tag{11}$$

where $\overline{u}$ is the bulk flow velocity.

Thus the radiative source term must be updated after N_{it} LES iterations such as :

$$N_{it} = \frac{\tau_f}{\Delta t_{LES}} = \frac{c_s}{0.7 \times \overline{u}} = \frac{1}{0.7M} \tag{12}$$

For the low-Mach flows considered here $N_{it} \sim 100$. The coupling frequency has also been studied on the same configuration by Dos Santos *et al.* [15, 3] who tested different values from 20 to 500. They also found $N_{it} = 100$ is the best compromise between accuracy and computing time. It is therefore retained for the following study.

3.3 CPU time synchronisation

Knowing the coupling frequency, the minimal CPU time is obtained if :

$$N_{it} \times t_{LES}^{CPU} = t_{Rad}^{CPU} \tag{13}$$

where t_{LES}^{CPU} et t_{Rad}^{CPU} are respectively the CPU time required for one fluid iteration and one radiative calculation. As both solvers are parallel, the restitution time for each code depends on the allocated number of processors :

$$\begin{aligned} t_{LES}^{CPU} &= \alpha(P_{LES}) \times t_{LES}^{CPU,1}/P_{LES} \\ t_{Rad}^{CPU} &= \alpha(P_{Rad}) \times t_{Rad}^{CPU,1}/P_{Rad} \end{aligned} \tag{14}$$

where $t_*^{CPU,1}$ is the CPU time for on 1 processor, P_* the number of allocated processors and $\alpha_*(P_*)$ the speed-up factor. For a code with a perfect speed-up this factor is equal to 1.

Combining Eqs. 13 and 14 and for a total number of processors $P = P_{LES} + P_{Rad}$, the final processor distribution is :

$$\begin{aligned} P_{LES} &= \frac{P}{(t_{Rad}^{CPU,1}/t_{LES}^{CPU,1})/N_{it} + 1} \\ P_{rad} &= P - P_{LES} \end{aligned} \tag{15}$$

AVBP is parallelized with a domain decomposition which is very efficient on massively parallel architectures with a perfect speed-up factor up to 4 078 processors on IBM BlueGene/L [39]. PRISSMA uses two levels of parallelization. The calculation of the absorption coefficients is parallelized with a domain decomposition as it depends on local flow quantities only. The integration of the incident intensity is also parallelized on the bands (for SNBcK model) and on the incident directions. As the integration of the incident intensity involves the whole domain the use of domain decomposition is not straightforward for radiation. By now the good scalability of PRISSMA is limited to the number of processor equal to the number of directions used for the DOM (i.e. the speed up factor is equal to 1 until 24 processors for an S_4 quadrature). This is a important limitation for coupled simulations on industrial configurations and the use of domain decomposition for radiation is currently investigated.

4 Optimal choice of models and discretization in the radiative solver

To evaluate the impact of the chosen discretization and spectral model on the radiative source term, a serie of calculations have been performed using one instantaneous flow solution. Fig. 6 shows the temperature field and the corresponding radiation source term S_r in the planes $y = 0$ and $z = 0$.

The optimal choice is a best compromise between accuracy and calculation time. Accuracy is estimated by the relative

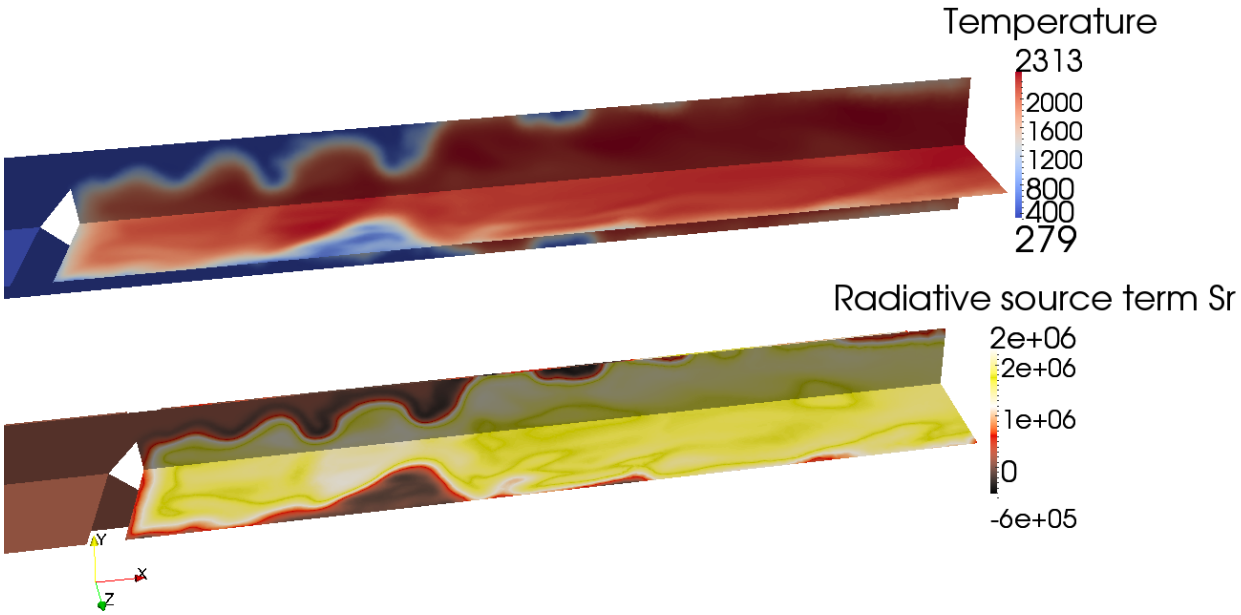

Fig. 6. Instantaneous fields of temperature and radiative source term S_r (W/m^3) in the $y = 0$ et $z = 0$ planes.

error compared to a reference solution for the total radiative energy:

$$\varepsilon_{\text{tot}} = \frac{|\langle\Psi\rangle - \langle\Psi_{ref}\rangle|}{\langle\Psi_{ref}\rangle} \tag{16}$$

where $\langle\Psi\rangle$ is the total radiated energy.

The mean relative error and its variance are also estimated along the central axis as:

$$\begin{aligned} \bar{\varepsilon} &= \frac{\overline{|S_r - S_{r,ref}|}}{\overline{S_{r,ref}}} \\ \sigma &= \sqrt{\overline{\varepsilon^2} - \bar{\varepsilon}^2} \end{aligned} \tag{17}$$

where the overline denotes the average along the central axis.

The calculation of radiation depends on the number of integration of the RTE integrations and the number of discretization points, It can be written as :

$$t_{Rad}^{CPU} \propto \underbrace{N_{dir}}_{\text{Angular discretisation}} \times \underbrace{N_{Bands} \times N_q}_{\text{Spectral model}} \times \underbrace{N_{Points}}_{Mesh} \tag{18}$$

In the next sections, the impact on the CPU time of each contributor (number of directions, spectral bands and mesh points) is discussed.

4.1 Angular quadrature

In DOM different quadratures may be used : S_N means $N(N+2)$ directions (S_4 : 24 directions), LC_{11} has 96 directions. A coarse angular discretization may lead to the so-called ray-effect that alters the solution accuracy. Previous studies have shown that LC_{11} is comparable to an exact Monte-Carlo approach [27, 14] and is used as a reference. Radiation source

Quadrature	Total radiative energy (W)	ε_{tot} (%)	Error on central profile (%)	
			$\bar{\varepsilon}$	σ
LC_{11}	1 326.31	–	–	–
S_4	1 319.65	0.5	1.14	0.67

Table 2. Accuracy on the total radiative energy ε_{tot} and on the radiative source term along the central axis $\bar{\varepsilon}$, σ of the angular quadrature on the radiative solution using FS-SNBck$_{15}$, the relative error is calculated against LC_{11} solution.

terme obtained along the central axis with the S_4 quadrature is compared to the LC_{11} result in Fig. 7 both using the global model FS-SNBcK$_{15}$ ($N_q = 15$). The relative error ε of S_4 compared to LC_{11} is weak, with a maximum of 2.86% along the central axis (Table 2). The total radiative energy obtained with the S_4/FS-SNBcK$_{15}$ model is 1319.65 *W* and is close to the LC_{11}/FS-SNB-cK$_{15}$, reference value of 1326.31 with an error of 0.5%. The recent study by Zhang *et al.* [40] on the same configuration, comparing the S_4 solution with a Monte-Carlo solution also confirms the good accuracy of the S_4 quadrature.

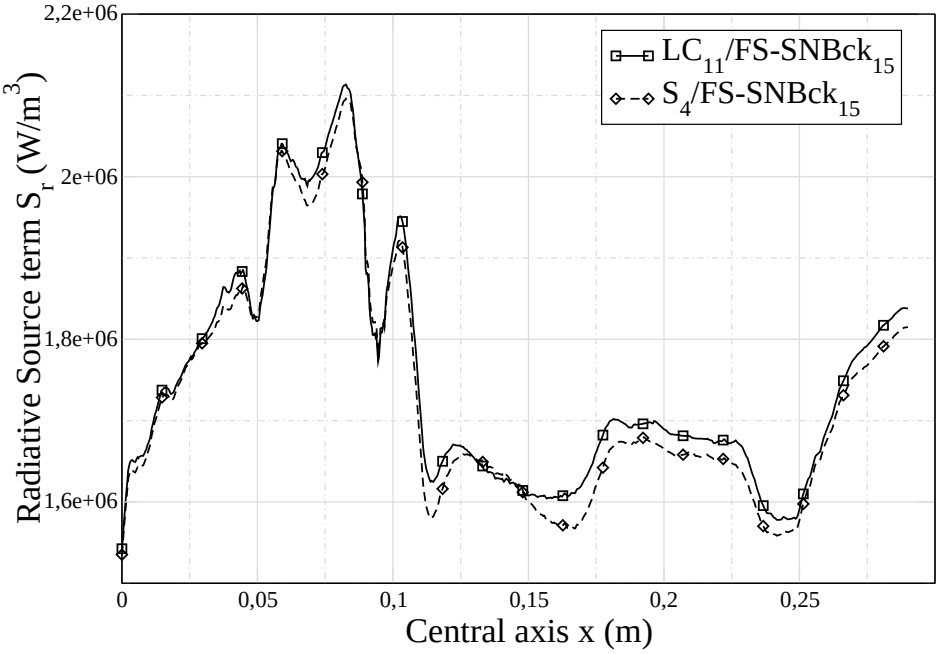

Fig. 7. Radiative source terme along the central axis for the LC_{11} (96 directions) and the S_4 (24 directions) angular discretization.

4.2 Spectral model

The choice of the spectral model is a key point to decrease the CPU time of radiation. The number of integrations of the RTE is proportional to the number of band and quadrature points from 1 800 integrations in the SNBcK model to only 3 to 15 integrations are sufficient for global models (WSGG, FS-SNBcK).

The results on the radiative source term in Fig. 8 show a strong discrepancy between the WSGG solution and the SNBcK : S_r is underestimated by more than 40%. Remember that the WSGG model is tabulated for the perfect combustion of methane with a constant ratio $X_{CO_2}/X_{H_2O} = 1/2$. In the case of propane this ratio is $3/4$, so that the absorption of CO_2 is underestimated by a factor $2/3$ which could explain the error on S_r.

The accuracy of FS-SNBcK depends mainly on the number of quadrature points [34] which is confirmed in Fig. 8. The solution with $N_q = 15$ agrees very well with the SNBcK solution with a maximum error ε of 4.7% along the central axis

while using only $N_q = 7$ leads to significant errors of 20%. However the CPU time associated to FS-SNBcK still remains important compared to WSGG and must be reduced.

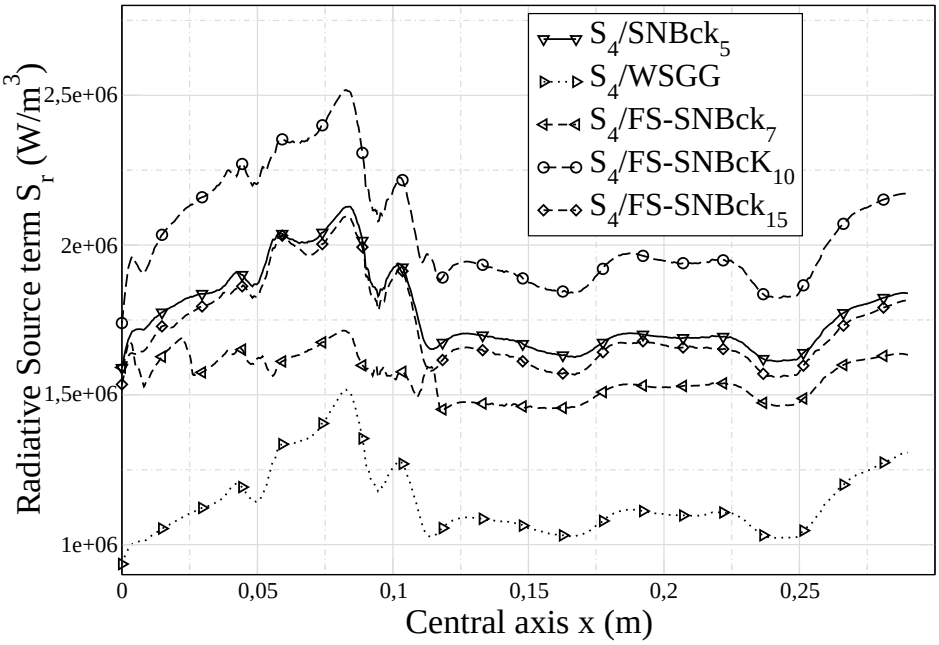

Fig. 8. Radiative source term for different spectral models along the central axis : SNBcK ($N_q = 5$), FS-SNBcK for $N_q = 7, 10, 15$ and WSGG.

This is achieved by using a tabulation of the FS-SNBcK model [25], where the absorption coefficient is tabulated for temperature and molar fraction steps : $\Delta T = 5$ K, $\Delta X_{H_20} = \Delta X_{CO_2} = \Delta X_{CO} = 0.02$. This allows to reach WSGG calculation times and will be detailed in a future paper . The maximal molar fractions obtained in LES ($X_{H_2O,max} = 0.18$, $X_{CO_2,max} = 0.13$ and $X_{CO,max} = 0.04$), allow to keep the table size small (38 Mb in ascii format for $Nq = 15$). In Fig. 9, the tabulated FS-SNBcK result is compared to the SNBcK and the WSGG solutions, showing a mean error ε on the central profile of 4.03% at CPU cost similar to WSGG.

Table 3 summarizes the errors on radiative energies for each spectral model compared to SNBcK taken as a reference. The WSGG model leads to an important error of 32% on the total energy while the error obtained for tabulated FS-SNBcK$_{15}$ is only 4%. It can be noticed in Table 3 that because of the spatial averaging over the domain the error on the total radiative energy is smaller in the tabulated case than in the FS-SNBck$_{15}$ but the errors on the central profile are higher.

5 Influence of the temporal and spatial resolutions

The temporal resolution has been discussed in section 3.2. To validate the coupling frequency $N_{it} = 100$, profiles of S_r are plotted along the central axis in Fig. 10 at $t = t_1$, $t = t_1 + 100\Delta t_{LES}$ and from a mean solution over $[t_1;t_1 + 100\Delta t_{LES}]$. All the results are very close, nearly merged. The retained coupling frequency $\Delta t_{Rad} = 100\Delta t_{LES}$ is then well justified and the temperature and molar fraction fluctuation within 100 fluid iterations do not impact S_r.

Radiation is impacted by the turbulence through the so-called Turbulence Radiation Interaction (TR)I [10]. The influence of the spatial resolution must then be checked for coupling combustion and radiation. Subgrid scale fluctuations may also impact radiation in principle but previous studies of TRI in the LES context [41,42,1,43] have shown that subgrid fluctuations can be neglected.

An other problem linked to grid resolution is the memory occupancy as domain decomposition can not be easily applied to radiation, which requires that properties over the whole domain must be known at each point, i.e. must be available in all processors. On the LES grid, presented in the section 1.1, the memory occupancy for the radiative solver is more than 4 Gb

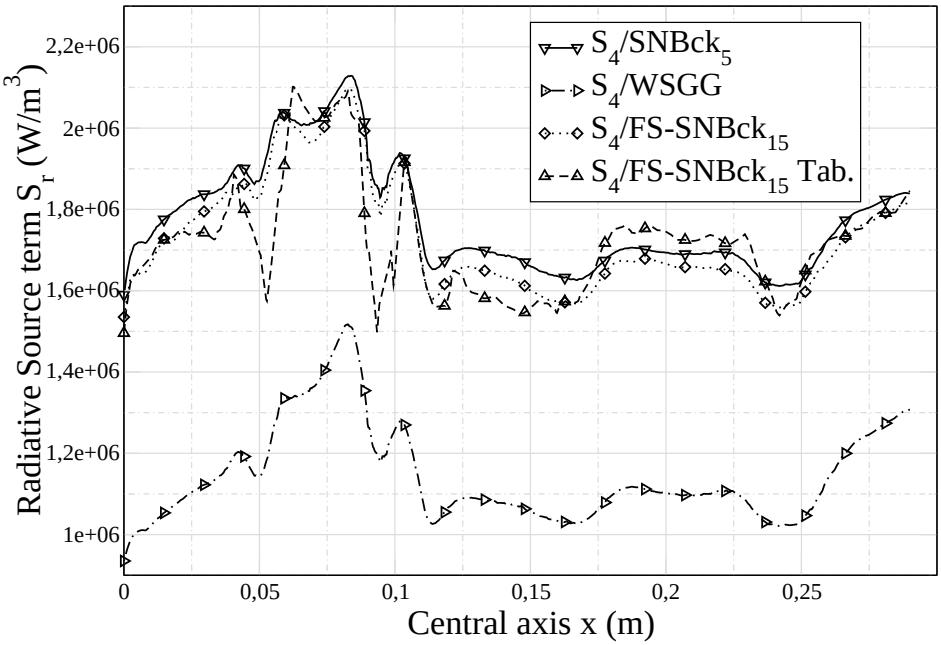

Fig. 9. Influence of the tabulation for the FS-SNBcK model with $N_q = 15$.

Spectral model	Total radiative energy (W)	ε_{tot} (%)	Errors on central profile (%) $\bar{\varepsilon}$	σ
SNBcK	1 396.92	–	–	–
WSGG	941.92	32.57	35.49	2.82
FS-SNBcK$_7$	1 262.02	9.66	11.99	3.93
FS-SNBcK$_{10}$	1 517.75	8.65	15.23	1.91
FS-SNBcK$_{15}$	1 319.65	5.53	2.45	0.88
FS-SNBcK$_{15}$ Tab.	1 339.81	4.09	4.03	3.36

Table 3. Accuracy on the total radiative energy ε_{tot} and on the radiative source term along the central axis $\bar{\varepsilon}$, σ of the spectral model on the radiative solution, the relative error is calculated against SNBcK solution.

(Table 4), i.e. twice the available memory on the used computed (IBM JS21, 56 nodes quadcore Power5+@1.5 GHz, 8 Gb memory, i.e. 2 Gb/core). The only way to reduce the memory occupancy is to coarser the mesh. Of course this should not alters the accuracy of the solution.

This is possible as the flow solver required very fine mesh to describe the turbulent flow in regions that are otherwise homogeneous in temperature and composition, i.e. where radiation exchanges are null. From the results of Poitou *et al.* [41], the impact of fluid variables fluctuations on radiation can be characterized and used to coarsen the mesh in regions where the temperature is sufficiently homogeneous while keeping small cells sizes where the temperature is fluctuating. This is based on the average temperature field and its variance are illustrated plotted in Fig. 11 in the $y = 0$ plane.

To evaluate the dependence of the accuracy of the solution on the mesh resolution , 3 grids have been tested. The original mesh (Grid 0) contains 4 744 561 cells with a cell size of 1 mm close to the flame holder. Starting from Grid 0 and using the average temperature fields, two meshes have been built, shown in Fig. 12. The grids keep the cells as small as possible where temperature RMS (Root Main Square) is important (Fig. 11), while the size of the cells is increased to about 1 cm in the fresh gases zone where there is no absorption (only the absorption of CO_2, H_2O, CO are considered here). Grid 1 contains

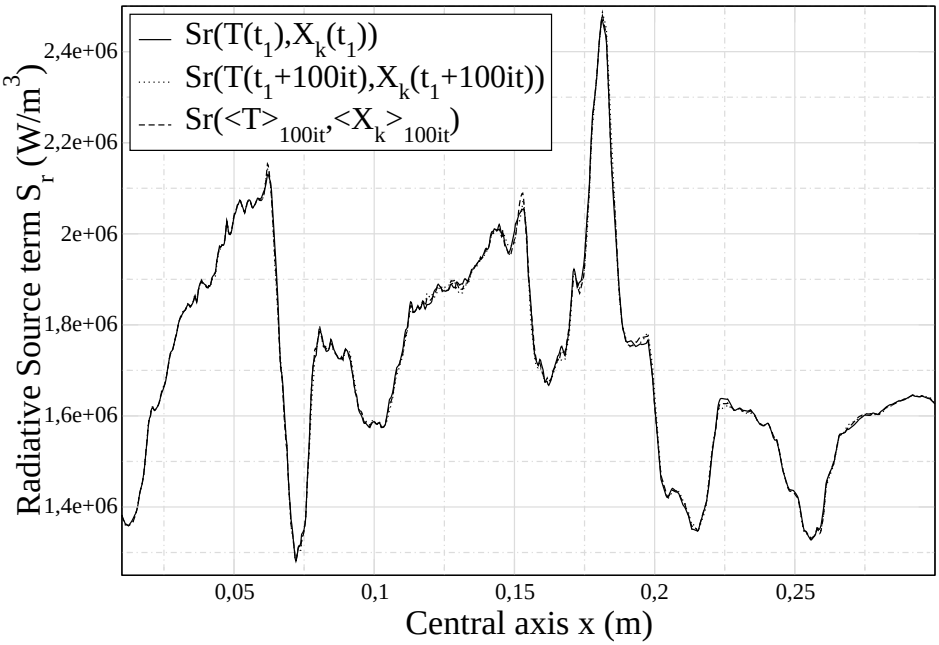

Fig. 10. Radiative source term along the central axis, calculated at t_1, $t_1 + 100it$ and with the time averaged variables over 100 iterations.

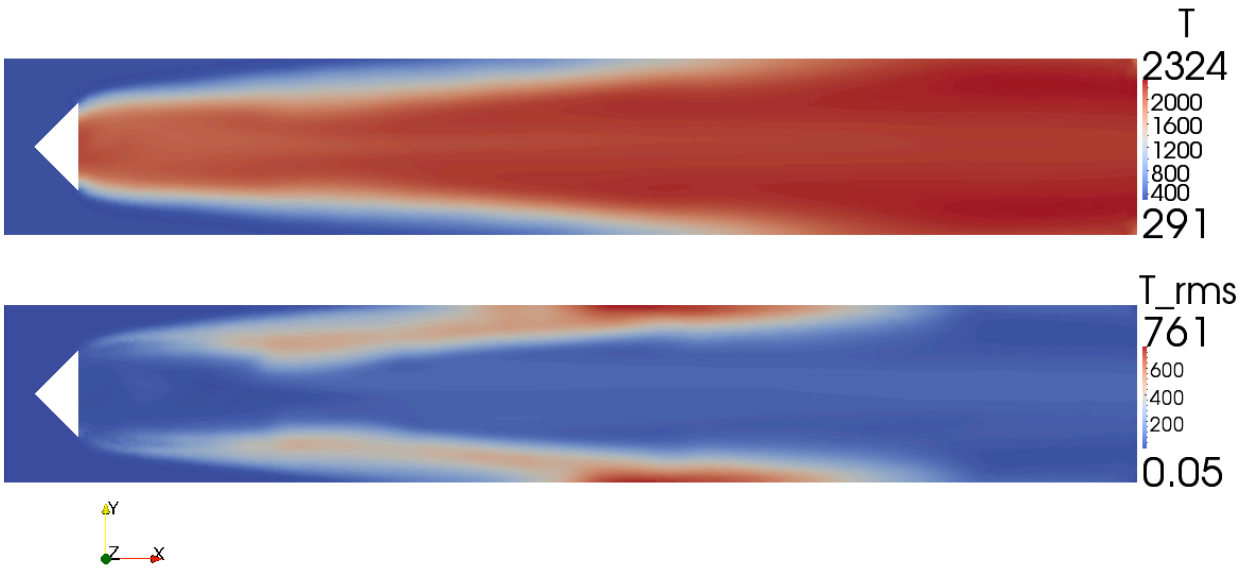

Fig. 11. Mean and RMS temperature fields in $y = 0$ plane.

2 500 560 cells, and has the same cell size as Grid 0 (1 mm) in the temperature fluctuating zone. Grid 2 contains 621 167 cells and has cells twice the size of Grid 0 (2 mm) in the temperature fluctuating zone. The associated memory occupancy is given in Table 4 : it decreases linearly with the cell number.

Al grids must guarantee optically thin cells as required by the Diamond Mean Flux Scheme (DMFS) used in PRISSMA [2] to avoid numerical scattering, so-called “false-scattering”. Using the mean Planck absorption coefficient to a criterion for the maximal cell size as : $\kappa_P \Delta x \leq 0.1$. Fig. 13 shows κ_P for the mean solution in the range $[0; 1.47]\mathrm{m}^{-1}$ which gives a maximum cell size of 7cm, far above the cell size in all grids.

	Number of cells	Master	Slave
Grid 0	4 744 561	4 500 Mb	3 378 Mb
Grid 1	2 500 560	2 246 Mb	1 605 Mb
Grid 2	621 167	620 Mb	478 Mb

Table 4. Memory occupancy for the radiative solver PRISSMA for different meshes.

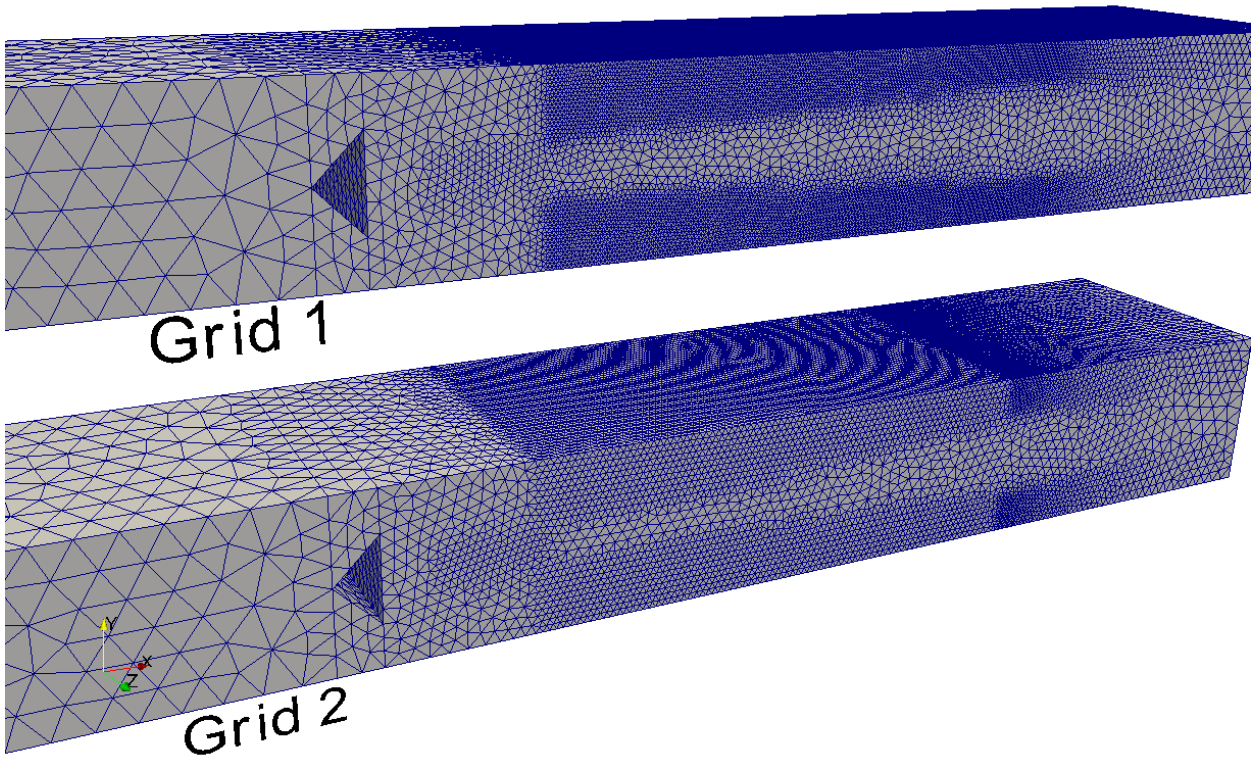

Fig. 12. Grid 1 where the cell size cell in the fluctuating zone of temperature is kept constant a in the original mesh (1 mm). Grid 2 where the cell size in the fluctuating zone of temperature is twice the original mesh (2 mm).

Fig. 13. Mean Planck absorption coefficient (m^{-1}) from the temporally averaged solution $\langle T \rangle$, $\langle X_i \rangle$ in the plane $z = 0$.

The influence of the mesh is illustrated along the central axis and the transversal axis at $x = 9$ cm in Figs. 14 and 15. Although some differences appear on S_r profiles along the central axis, they are very small along the transversal axis for the 3 grids. The total radiative energies are 1304.35 W and 1301.75 W for respectively Grid 1 and 2, which represents a relative error of 1.16% and 1.36% if compared to the original mesh (Table 5), which is smaller than the error due to the spectral model (section 4.2).

This result confirms previous studies on TRI [41, 42, 1, 43] conducted *a priori* in academic configurations that the

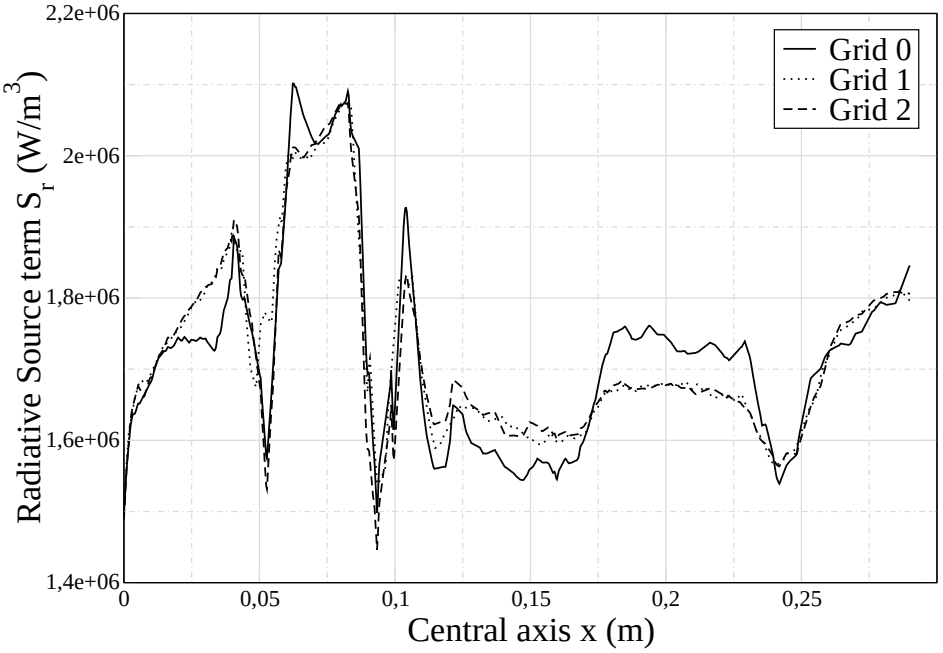

Fig. 14. Radiative source term along the central axis, calculated with FS-SNBcK model, $N_q = 15$, S_4 with black walls (no reflection) for the 3 grids.

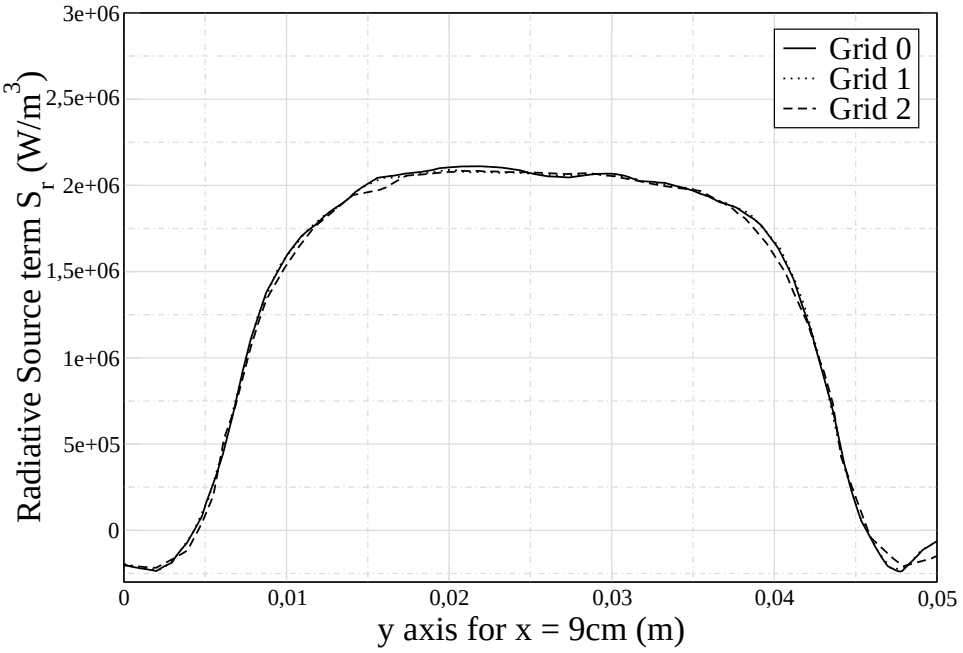

Fig. 15. Radiative source term along the y axis ($x = 9$ cm), calculated with FS-SNBcK model, $N_q = 15$, S_4 with black walls (no reflection) for the 3 grids.

Quadrature	Total radiative energy (W)	ε_{tot} (%)	Errors on central profile (%) $\bar{\varepsilon}$	σ
Grid 0	1 326.31	–	–	–
Grid 1	1 304.35	1.16	2.39	1.77
Grid 2	1 301.75	1.36	2.46	1.52

Table 5. Accuracy on the total radiative energy ε_{tot} and on the radiative source term along the central axis $\bar{\varepsilon}$, σ of grid resolution on the radiative solution using FS-SNBck$_{15}$, the relative error is calculated against Grid 0 solution.

influence on the radiation of subgrid scale fluctuation is small. Here the increase of the mesh size, between Grid 0 and 2, is equivalent to a spatial filtering with a filter size from $2\Delta x_{LES}$ to $10\Delta x_{LES}$. As ignoring the fluctuations smaller than $2\Delta x_{LES}$ give a maximal error of 1.36%, it is possible to conclude *a posteriori* no subgrid scale model is required for radiation in LES context.

6 Influence of the boundary conditions : reflective walls

From a radiative point of view, walls are characterized by a temperature and an emissivity. The ceramic wall emissivity is $\varepsilon = 0.91$ [3]. The flame holder emissivity is taken from for a stainless steels lightly oxidized at 1000 K, $\varepsilon = 0.4$ [3]. The inlet, outlet and the atmosphere are assumed to be black enclosures (*i.e.* all incident radiation is absorbed).

Quartz windows are semi-transparent, i.e. their emissivity is a function of the wavelength (Fig. 16). This is a particularity of the experimental configuration as in a real combustor there are no transparent walls. The quartz spectral emissivity shown in Fig. 16 [3] was provided by the manufacturer for the interval $[0.5;4.5\ \mu m]$ and results from an emissivity calculation based on the complex index of the medium [44] for the interval $[4.5;15\ \mu m]$. It is assumed to be 1 in the interval $[15;68\ \mu m]$. To describe the quartz emissivity in global spectral models the mean emissivity (weighted by the Planck function) over the full spectrum is calculated. Using the temperature of 300 K, the mean quartz emissivity is $\varepsilon = 0.879$ even for the SNBcK case.

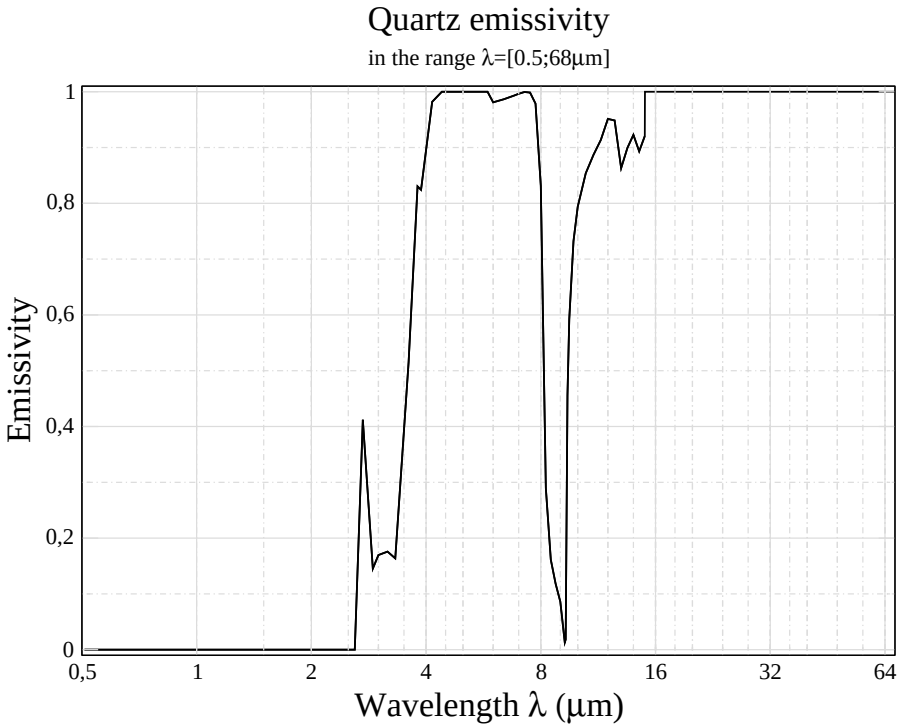

Fig. 16. Quartz spectral emissivity.

Spectral model	Total radiative energy (W)	ε_{tot} (%)
SNBcK	1331.47	4.69
WSGG	900.92	4.94
FS-SNBcK$_{15}$	1254.49	4.93
FS-SNBcK$_{15}$, Tab.	1273.82	4.35

Table 6. Relative difference ε_{tot} on the total radiative energy for different spectral models compared to the cases without reflection.

The influence of reflection has been evaluated using S_4 calculations on Grid 2 and for different spectral models. Results along the central axis are shown in Fig. 17 for the SNBcK model and shows that the influence of the reflection is limited on the radiative source term. Tests with global models gave similar results as in Table 6 where the relative difference of the calculations with ans without reflection is given. All spectral models give a similar result and a relatively small difference around 5%. The conclusion is different for the radiative heat flux to the wall. Fig. 18 shows the wall radiative flux at the upper wall ($y = 2.5$cm). The flux is increased by one order of magnitude when the reflection is included. As the medium is optically thin, exchanges due to multiple reflections can arise between walls and add up to significantly increase wall fluxes.

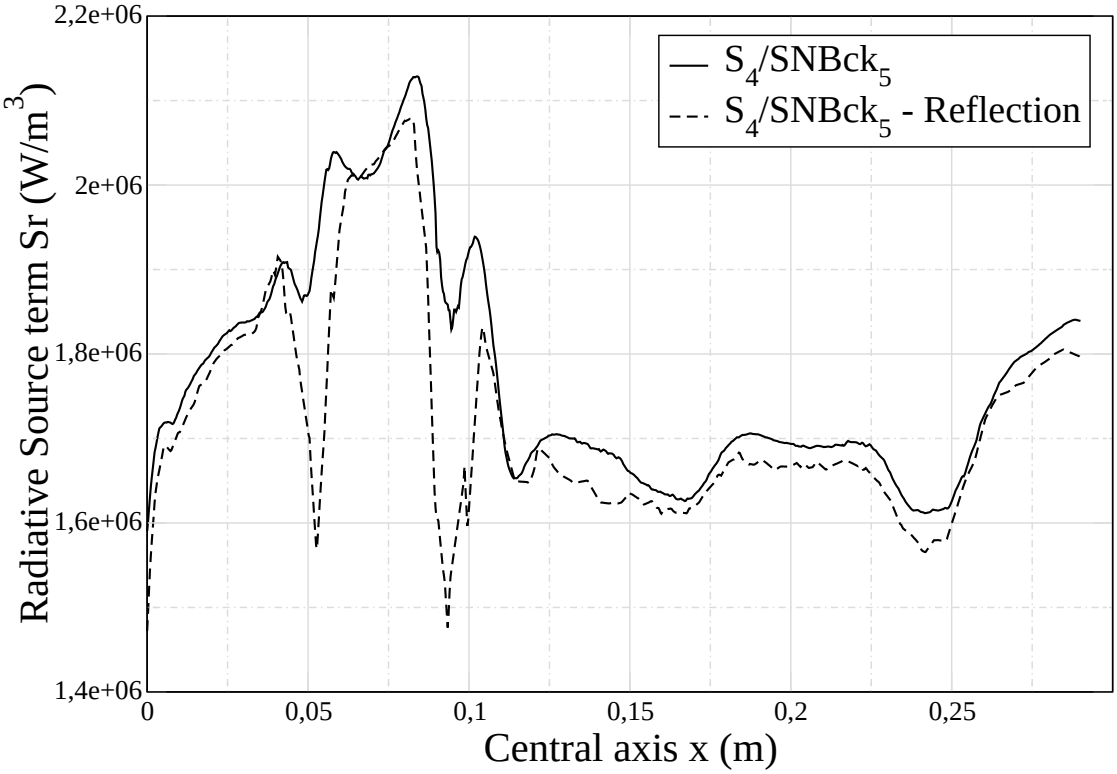

Fig. 17. Radiative source term along the central axis for the SNBcK model on the Grid 2 with an S_4 quadrature. Line : without reflection, dashed : with reflection.

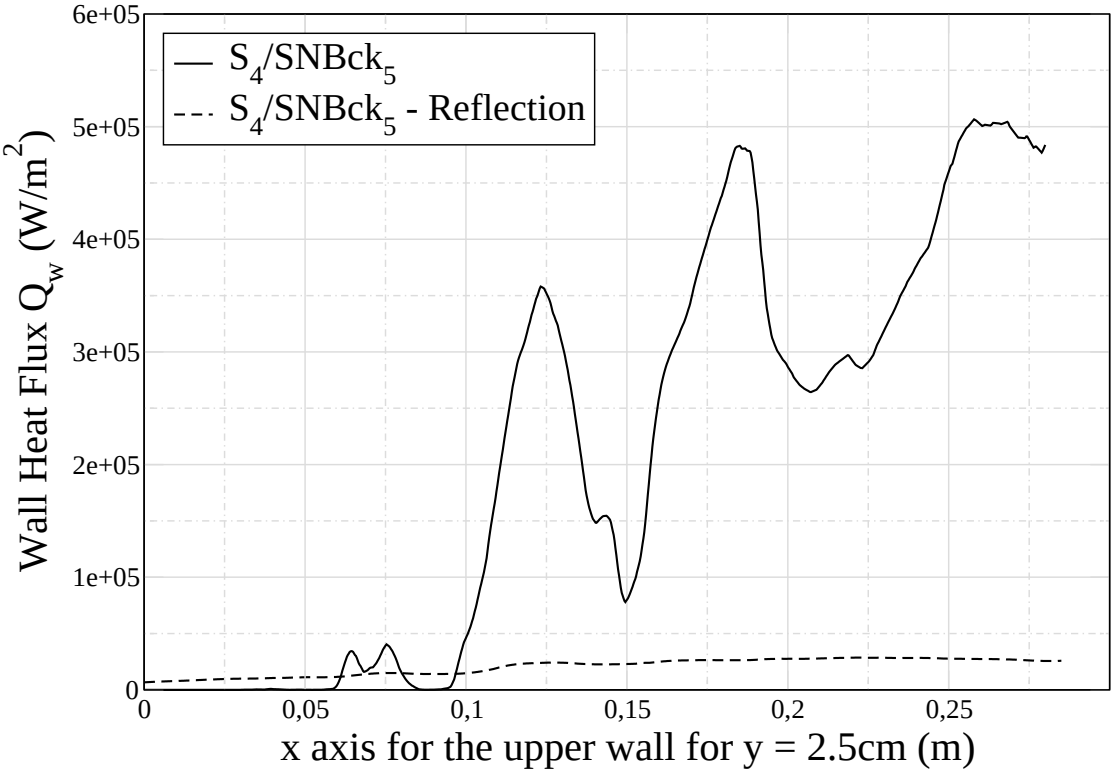

Fig. 18. Wall radiative flux along the x axis at $y = 2.5$ cm et $z = 0$ (quartz wall) for the SNBcK model on Grid 2 with an S_4 quadrature. Line : without reflection, dashed : with reflection.

7 Summary of calculation time and accuracy

The performance in terms of accuracy and computing time of the radiative solver with all possible models and discretizations are summarized in Table 7. The calculation times is given for a parallel calculation on 24 Intel(R) Xeon(R) CPU @ 2.66 GHz processors.

The radiative calculation time is split into 2 contributions, corresponding to spectral calculations (calculation of the absorption coefficient) and the geometrical calculations (integration of the RTE). The total time is the sum of both contributions plus the communication time and data I/O time.

As the absorption coefficients are functions of local variables the spectral calculation is parallelized with a domain decomposition method. WSGG and tabulated FS-SNBcK models use tabulated absorption coefficients the spectral time is negligible for these cases. The spectral calculation time is longer for the FS-SNBcK model than the SNBcK model because of the numerical inversion of the full spectrum cumulative function [34].

The geometrical time for all global models is much reduced compared to the SNBcK because the decrease of the number of resolutions of the RTE. Because of prohibitive CPU time, the LC_{11}/$SNBcK_5$ and S_4/$SNBcK_5$ with reflection calculation times are only estimated. Grid reduction is also very efficient in reducing the calculation time linearly with the number of cells.

Finally, including reflection increases the geometrical time increases by a factor 3 to 4 (the resolution of the RTE has been iterated 3 or 4 times to reach the convergence). Obviously global models should be used if the reflection is considered as the geometrical time is small compared to the use of SNBcK.

The accuracy of the solution is estimated from the total radiative energy calculated in Tables 2, 3 and 5. The total error is the sum of the errors linked to spectral model, angular quadrature and grid resolution. As an example, the error of the solution WSGG/S_4 on the mesh 1 is : 32.57 (Tab. 3) $+1.16$ (Tab. 5) $+0.5$ (Tab. 2) $= 34.23\%$. Solutions with an error above 10% are considered unacceptable. Clearly all WSGG calculations are not sufficiently accurate, while all SNBcK are always excellent even on the coarser mesh and FS-$SNBcK_{15}$ are good on all meshes.

Grid	Angular Quadrature	Spectral Model (Reflection)	Spectral time (s)	Geometrical time (s)	Total time (s)	PRISSMA/AVBP (TTGC)	Cumulated errors (%)
Grid 0	LC_{11}	$SNBck_5$ (estimated)	502,84	104 753,64	105 256,49	494,41	-
Grid 0	S_4	$SNBck_5$	502,84	26 188,41	26 691,26	125,37	0,5
Grid 0	LC_{11}	$SNBck_5$ – Reflection (estimated)	502,84	314 260,93	314 763,78	1 478,52	-
Grid 0	S_4	$SNBck_5$ – Reflection (estimated)	502,84	78 565,23	79 068,08	371,40	0,5
Grid 0	LC_{11}	$FS\text{-}SNBck_{15}$	4 022,75	876,05	4 931,88	23,17	5,53
Grid 0	S_4	$FS\text{-}SNBck_{15}$	4 022,75	219,01	4 269,89	20,06	6,03
Grid 0	S_4	$FS\text{-}SNBck_{15}$ Tab.	21,25	200,47	239,90	1,13	4,59
Grid 0	S_4	$FS\text{-}SNBck_{10}$	2 062,87	146,01	2 208,88	10,38	9,15
Grid 0	S_4	$FS\text{-}SNBck_{7}$	1 433,50	102,21	1 535,70	7,21	10,16
Grid 0	S_4	WSGG	6,19	39,61	89,27	0,42	33,07
Grid 1	S_4	$FS\text{-}SNBck_{15}$	1 572,41	107,67	1 919,53	9,02	7,19
Grid 1	S_4	WSGG	3,26	21,93	41,63	0,20	34,23
Grid 2	S_4	$SNBck_5$	442,61	4 863,08	12 049,66	56,60	1,86
Grid 2	S_4	$FS\text{-}SNBck_{15}$	395,84	25,75	482,30	2,27	7,39
Grid 2	S_4	$FS\text{-}SNBck_{15}$ Tab.	5,32	25,55	36,76	0,17	5,95
Grid 2	S_4	WSGG	0,81	5,19	9,70	0,05	34,43
Grid 2	S_4	$SNBck_5$ – Reflection	469,47	20 903,66	46 990,05	220,72	1,86
Grid 2	S_4	$FS\text{-}SNBck_{15}$ – Reflection	393,05	46,71	692,41	3,25	7,39
Grid 2	S_4	$FS\text{-}SNBck_{15}$ Tab. – Reflection	2,25	66,10	132,88	0,62	5,95
Grid 2	S_4	WSGG – Reflection	0,81	12,71	17,84	0,08	34,43

AVBP	Time for N_{it}=100 iterations	**# cells**	Ratio
Lax-Wendroff	106,45	4 744 561	1
TTGC	212,89	2 500 560	1,9
		621 167	7,64

Number of processors: 24

Reference solution
Acceptable precision
Unacceptable precision
LC11 : 96 directions
S4 : 24 directions

Table 7. Radiative calculation times for set of parameters, obtained on 24 processors Intel(R) Xeon(R) CPU @ 2.66 GHz.

In the PCS coupling (section 3.1), the radiation calculation time must be compared to the combustion CPU time for 100 iterations over 24 processors. This time is 106 *s* with the 2nd order spatial scheme (Lax-Wendroff) and 212 *s* with the 3rd order spatial scheme (TTGC) in the AVBP solver. In the case where the same number of processors is allocated to the fluid and the radiation solver the ratio of calculation times PRISSMA/AVBP (for the TTGC scheme) is given in the 7th column of Table 7. These ratio are sorted by decreasing in Fig. 19. Good solution correspond to a ratio less than 1, meaning that a coupled simulation cost or less than CPU of uncoupled calculation.

The reference solutions reach ratios up to 1 400. The ratio for S_4/SNBcK on Grid 0 without reflection is 125 which is still unacceptable. The tabulated $FS\text{-}SNBck_{15}/S_4$ calculation on Grid 2 gives an efficient ratio of 0.17.

The tabulated $FS\text{-}SNBck_{15}/S_4$ on Grid 2 with reflection is the optimum case, ensuring both rapidity and accuracy. The error on the total radiative energy is 5.95% which is acceptable in comparison to the precision of LES calculations. This optimum demonstrated that using global spectral models with reflection and sufficient number of discrete directions is more accurate than narrow band models where the high CPU cost imposes to neglect reflection or decrease the number of directions.

8 Conclusion

With the objective of coupled combustion-radiation simulations, a premixed turbulent flame has been studied from a radiative point of view to evaluate the efficiency and accuracy of the radiative solver.

A study of the models and discretization used in the radiative solver have been conduced on the angular quadrature, the spectral model and the spatial/temporal discretization. It has been demonstrated the spectral model is the most important

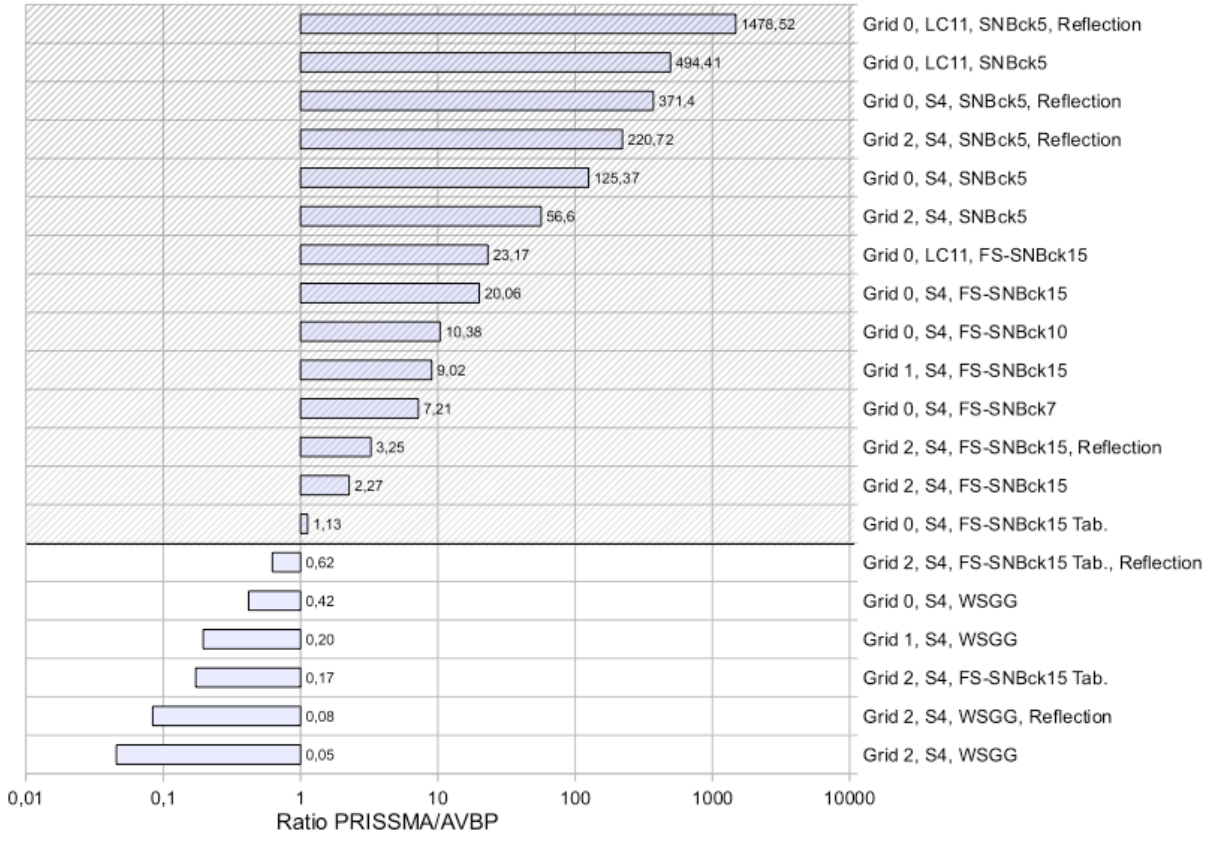

Fig. 19. Ratio of calculation times PRISSMA/AVBP for the different models and discretisations of the radiative solver.

parameter for combustion applications both for accuracy and CPU time.

The systematic comparison of the different parameters and choice of radiative models in terms of precision and cost demonstrate that a tabulated FS-SNBcK$_{15}$/S$_4$ on the coarsest grid and including reflection is the optimal combination. The radiative calculation time is then 350 times shorter than a SNBcK/S$_4$ calculation on the original mesh, and introduces an error less than 6%. With this model it is possible to obtain a radiative solution within a time 0.6 times shorter than 100 combustion iterations, the objective of reaching a CPU time ratio PRISSMA/AVBP less than one.

A mesh reduction has been applied to reduce the radiative calculation time and the memory occupancy of the radiative solver following the criterion of temperature fluctuations. It can be concluded that the radiative grid is larger than the fluid mesh. Mesh convergence confirms *a posteriori* the small influence of the LES subgrid scale fluctuations on radiation, and there is no need for subgrid models for radiation in LES.

An other important result is that it is possible to take into account reflection if a global spectral model is used. If the influence of reflection on the radiative source term is small, it remains very important for the radiative wall fluxes.

This work constitutes a first step toward coupled CFD-radiation simulations selecting the optimal methodology based on systematic comparisons. Coupled simulation are underway and the analysis of the influence of radiation on combustion will be discussed in a future paper.

References

[1] Coelho, P. J., 2009. "Approximate solutions of the filtered radiative transfer equation in large eddy simulations of turbulent reactive flows". *Combustion and Flame,* **156**(5), May, pp. 1099–1110. 1, 11, 14

[2] Joseph, D., 2004. "Modélisation des transferts radiatifs en combustion par méthode aux ordonnées discrètes sur des maillages non structurés tridimensionnels". PhD thesis, Institut National Polytechnique de Toulouse. 1, 6, 13

[3] dos Santos, R. G., 2007. "Large eddy simulation of turbulent combustion including radiative heat transfer". PhD thesis, EM2C. 1, 2, 4, 5, 8, 16

[4] Sagaut, P., 1998. *Introduction à la simulation des grandes échelles pour les écoulements de fluide incompressible*. Mathématiques & Applications, Vol. 30. 1

[5] Poinsot, T., and Veynante, D., 2001. *Theorical and Numerical Combustion*. Edwards. 1

[6] Boileau, M., Staffelbach, G., Cuenot, B., Poinsot, T., and Bérat, C., 2008. "LES of an ignition sequence in a gas turbine engine". *Combustion and Flame,* **154**(1-2), pp. 2–22. 1

[7] Nottin, C., Knikker, R., Boger, M., and Veynante, D., 2000. "Large eddy simulations of an acoustically excited turbulent premixed flame". *Symposium (International) on Combustion,* **28**(1), pp. 67–73. 1, 2

[8] Roux, A., Gicquel, L., Sommerer, Y., and Poinsot, T., 2008. "Large eddy simulation of mean and oscillating flow in side-dump ramjet combustor". *Combustion and Flame,* **152**(1-2), pp. 154–176. 1

[9] Boudier, G., Gicquel, L., and Poinsot, T., 2008. "Effects of mesh resolution on large eddy simulation of reacting flows in complex geometry combustors". *Combustion and Flame,* **155**, pp. 196–214. 1

[10] Coelho, P. J., 2007. "Numerical simulation of the interaction between turbulence and radiation in reactive flows". *Progress in Energy and Combustion Science,* **33**(4), Aug., pp. 311–383. 2, 11

[11] Desjardin, P. E., and Frankel, S. H., 1999. "Two-dimensional large eddy simulation of soot formation in the near-field of a strongly radiating nonpremixed acetylene-air turbulent jet flame". *Combustion and flame,* **119**(1-2), pp. 121–132. 2

[12] Jones, W., and Paul, M., 2005. "Combination of DOM with LES in a gas turbine combustor". *International Journal of Engineering Science,* **43**(5-6), Mar., pp. 379–397. 2

[13] Joseph, D., Hafi, M. E., Fournier, R., and Cuenot, B., 2005. "Comparison of three spatial differencing schemes in discrete ordinates method using three-dimensional unstructured meshes". *International Journal of Thermal Sciences,* **44**(9), Sept., pp. 851–864. 2, 6

[14] Joseph, D., Perez, P., Hafi, M. E., and Cuenot, B., 2009. "Discrete Ordinates and Monte-Carlo Methods for radiative transfer simulation applied to computational fluid dynamics combustion modeling". *Journal of Heat Transfer,* **131**(5), May, pp. 052701–9. 2, 6, 9

[15] dos Santos, R. G., Lecanu, M., Ducruix, S., Gicquel, O., Iacona, E., and Veynante, D., 2008. "Coupled large eddy simulations of turbulent combustion and radiative heat transfer". *Combustion and Flame,* **152**(3), Feb., pp. 387–400. 2, 5, 8

[16] Knikker, R., Veynante, D., Rolon, J., and Meneveau, C., 2000. "Planar laser-induced fluorescence in a turbulent premixed flame to analyze Large Eddy Simulation models". In Proceedings of the 10th international Symposium on Applications of Laser Techniques to Fluid Mechanics. 2

[17] Knikker, R., Veynante, D., and Meneveau, C., 2002. "A priori testing of a similarity model for large eddysimulations of turbulent premixed combustion". *Proceedings of the Combustion Institute,* **29**(2), pp. 2105–2111. 2

[18] Colin, O., and Rudgyard, M., 2000. "Development of high-order Taylor-Galerkin schemes for LES". *Journal of Computational Physics,* **162**(2), pp. 338–371. 3, 7

[19] Ducros, F., Nicoud, F., and Poinsot, T., 1998. "Wall-adapting local eddy-viscosity models for simulations in complex geometries". In ICFD, B. M. J., ed., pp. 293–300. 3

[20] Nicoud, F., and Ducros, F., 1999. "Subgrid-scale stress modelling based on the square of the velocity gradient tensor". *Flow, Turbulence and Combustion,* **62**(3), pp. 183–200. 3

[21] Colin, O., Ducros, F., Veynante, D., and Poinsot, T., 2000. "A thickened flame model for large eddy simulations of turbulent premixed combustion part2". *Physics of Fluids,* **12**(7), pp. 1843–1863. 3

[22] Selle, L., Lartigue, G., Poinsot, T., Koch, R., Schildmacher, K.-U., Krebs, W., Prade, B., Kaufmann, P., and Veynante, D., 2004. "Compressible Large-Eddy Simulation of turbulent combustion in complex geometry on unstructured meshes". *Combustion and Flame,* **137**(4), pp. 489–505. 3

[23] Poinsot, T., and Lele, S., 1992. "Boundary conditions for direct simulations of compressible viscous flows". *Journal of Computational Physics,* **vol.101**(1), pp. 104–129. 3

[24] Amaya, J., 2010. "Unsteady coupled convection, conduction and radiation simulations on parallel architectures for combustion applications". PhD thesis, CERFACS. 4

[25] Poitou, D., 2009. "Modélisation du rayonnement dans la simulation aux grandes échelles de la combustion turbulente". PhD thesis, Institut National Polytechnique de Toulouse, Décembre. 5, 6, 11

[26] Joseph, D., Coelho, P. J., Cuenot, B., and Hafi, M. E., 2003. "Application of the discrete ordinates method to grey media in complex geometries using 3-dimensional unstructured meshes". In Eurotherm73 on Computationnal Thermal Radiation in Participating Media, Vol. 11, Eurotherm series, pp. 97–106. 6

[27] Jensen, K. A., Ripoll, J., Wray, A., Joseph, D., and Hafi, M. E., 2007. "On various modeling approaches to radiative heat transfer in pool fires". *Combustion and Flame,* **148**(4), Mar., pp. 263–279. 6, 9

[28] Truelove, J. S., 1987. *Discrete-ordinate solutions of the radiation transport equation.* 6

[29] Goutiere, V., Liu, F., and Charette, A., 2000. "An assessment of real-gas modelling in 2D enclosures". *Journal of Quantitative Spectroscopy and Radiative Transfer,* **64**, Feb., pp. 299–326. 6

[30] Goutière, V., Charette, A., and Kiss, L., 2002. "Comparative performance of non-gray gas modeling techniques". *Numerical Heat Transfer Part B: Fundamentals,* **41**, Mar., pp. 361–381. 6

[31] Soufiani, A., and Taine, J., 1997. "High temperature gas radiative propriety parameters of statistical narrow-band model for H_2O, CO_2 and CO and correlated-k model for H_2O and CO_2". *Technical note in International Journal of Heat and*

mass transfer, **40**, pp. 987–991. 6

[32] Soufiani, A., and Djavdan, E., 1994. "A comparison between weighted sum of gray gases and statistical narrow-band radiation models for combustion applications". *Combustion and Flame,* **97**(2), pp. 240 – 250. 6

[33] Liu, F., Yang, M., Smallwood, G., and Zhang, H., 2004. "Evaluation of the SNB based full-spectrum CK method for thermal radiation calculations in $CO_2 - H_2O$ mixtures". In Proceedings of ICHMT. 6

[34] Poitou, D., Amaya, J., Bushan Singh, C., Joseph, D., Hafi, M. E., and Cuenot, B., 2009. "Validity limits for the global model FS-SNBcK for combustion applications". In Proceedings of Eurotherm83 – Computational Thermal Radiation in Participating Media III. 6, 7, 10, 18

[35] Amaya, J., Cabrit, O., Poitou, D., Cuenot, B., and Hafi, M. E., 2010. "Unsteady coupling of Navier-Stokes and radiative heat transfer solvers applied to an anisothermal multicomponent turbulent channel flow". *Journal of Quantitative Spectroscopy and Radiative Transfer,* **111**(2), pp. 295–301. 7

[36] Duchaine, F., Corpron, A., Pons, L., Moureau, V., Nicoud, F., and Poinsot, T., 2009. "Development and assessment of a coupled strategy for conjugate heat transfer with Large Eddy Simulation. Application to a cooled turbine blade". *International Journal of Heat and Mass Transfer,* **submitted**. 7

[37] Leacanu, M., 2005. "Couplage multi-physique combustion turbulente - rayonnement - cinétique chimique". PhD thesis, École centrale Paris. 8

[38] Wang, Y., 2005. "Direct numerical simulation of non-premixed combustion with soot and thermal radiation". PhD thesis, University of Maryland. 8

[39] Staffelbach, G., Gicquel, L. Y. M., and Poinsot, T., 2007. *Highly Parallel Large Eddy Simulations of Multiburner Configurations in Industrial Gas Turbines*, Vol. Complex Effects in LES. pp. 325–336. Lecture Notes in Computational Science and Engineering. 8

[40] Zhang, J., Gicquel, O., Veynante, D., and Taine, J. "Monte carlo method of radiative transfer applied to a turbulent flame modeling with LES". *Comptes Rendus Mécanique,* **337**(6-7), pp. 539–549. 10

[41] Poitou, D., Hafi, M. E., and Cuenot, B., 2007. "Diagnosis of Turbulence Radiation Interaction in turbulent flames and implications for modeling in Large Eddy Simulation". *Turkish Journal of Engineering and Environmental Sciences,* **31**, pp. 371–381. 11, 12, 14

[42] Roger, M., Silva, C. B. D., and Coelho, P. J., 2009. "Analysis of the turbulence-radiation interactions for Large Eddy Simulations of turbulent flows". *International Journal of Heat and Mass Transfer,* **52**(9-10), pp. 2243 – 2254. 11, 14

[43] Roger, M., Coelho, P. J., and da Silva, C. B., 2010. "The influence of the non-resolved scales of thermal radiation in Large Eddy Simulation of turbulent flows: A fundamental study". *International Journal of Heat and Mass Transfer,* **53**(13-14), pp. 2897–2907. 11, 14

[44] Palik, E. D., and Ghosh, G., 1998. *Handbook of optical constants of solids*. Academic Press. 16